Assessment of Outer Retinal Remodeling in the Hibernating 13-Lined Ground Squirrel

Benjamin S. Sajdak,[1] Brent A. Bell,[2] Tylor R. Lewis,[1] Gabriel Luna,[3] Grayson S. Cornwell,[3] Steven K. Fisher,[3] Dana K. Merriman,[4] and Joseph Carroll[1,5,6]

[1]Cell Biology, Neurobiology and Anatomy, Medical College of Wisconsin, Milwaukee, Wisconsin, United States
[2]Cole Eye Institute/Ophthalmic Research, Cleveland Clinic, Cleveland, Ohio, United States
[3]Neuroscience Research Institute, University of California Santa Barbara, Santa Barbara, California, United States
[4]Biology & Microbiology, University of Wisconsin Oshkosh, Oshkosh, Wisconsin, United States
[5]Ophthalmology & Visual Sciences, Medical College of Wisconsin, Milwaukee, Wisconsin, United States
[6]Biophysics, Medical College of Wisconsin, Milwaukee, Wisconsin, United States

Correspondence: Joseph Carroll, Department of Ophthalmology & Visual Sciences, Medical College of Wisconsin, 925 N 87th Street, Milwaukee, WI 53226-0509, USA; jcarroll@mcw.edu.

Submitted: October 7, 2017
Accepted: April 20, 2018

Citation: Sajdak BS, Bell BA, Lewis TR, et al. Assessment of outer retinal remodeling in the hibernating 13-lined ground squirrel. *Invest Ophthalmol Vis Sci*. 2018;59:2538–2547. https://doi.org/10.1167/iovs.17-23120

Purpose. We examined outer retinal remodeling of the euthermic and torpid cone-dominant 13-lined ground squirrel (13-LGS) retina using optical coherence tomography (OCT) imaging and histology.

Methods. Retinas and corneas of living 13-LGSs were imaged during euthermic and torpid physiological states using OCT. Retinal layer thickness was measured at the visual streak from registered and averaged vertical B-scans. Following OCT, some retinas were collected immediately for postmortem histologic comparison using light microscopy, immunofluorescence, or transmission electron microscopy.

Results. Compared to OCT images from euthermic retinae, OCT images of torpid retinae revealed significantly thicker inner and outer nuclear layers, as well as increases in the distances between outer retinal reflectivity bands 1 and 2, and bands 3 and 4. A significant decrease in the distance between bands 2 and 3 also was seen, alongside significant thinning of the choriocapillaris and choroid. OCT image quality was reduced in torpid eyes, partly due to significant thickening of the corneal stroma during this state.

Conclusions. The torpid retina of the hibernating 13-LGS undergoes structural changes that can be detected by OCT imaging. Comparisons between in vivo OCT and ex vivo histomorphometry may offer insight to the origin of hyperreflective OCT bands within the outer retina of the cone-dominant 13-LGS.

Keywords: ground squirrel, optical coherence tomography, hibernation, cone photoreceptors, choroid, cornea

Optical coherence tomography (OCT) provides real-time cross-sectional imaging of the retina and has grown to be a standard of ophthalmic care in humans.[1,2] Despite the impact of OCT on clinical care, questions remain about the anatomical origin of reflective signals visualized in OCT images of the outer retina. The International Nomenclature for Optical Coherence Tomography Panel has described the four hyperreflective outer bands visible in humans as the external limiting membrane (ELM), inner segment ellipsoid zone (EZ), photoreceptor outer segment (OS) and RPE contact region, called the interdigitation zone (IZ); and the RPE/Bruch's membrane complex.[3] These anatomical assignments are based largely on a model developed by reviewing human histology literature.[4] Some designations remain controversial: adaptive optics (AO)-OCT suggests that the EZ band instead corresponds to an inner segment (IS)/OS junction, and that the IZ band instead corresponds to cone or rod OS tips.[5,6] It is critical that we establish a complete understanding of how reflectivity is related to underlying photoreceptor structure as there often is a disconnect between the appearance of residual photoreceptor structure in diseased retinas across imaging modalities,[7–9] and EZ outcome measures are being used in clinical trials[10,11] despite the lack of consensus of the anatomical origin of the EZ band. This controversy is difficult to solve using human subjects, primarily due to challenges of obtaining samples for histologic correlation and the variability in outer segment length[12] and rod/cone topography[13] of visually normal patients. We reasoned that a cone-rich rodent model may overcome these limitations and provide valuable insight to the anatomical correlates of outer reflective bands in OCT images of the human macula.

The diurnal 13-lined ground squirrel (13-LGS) has a cone-rich retina that is amenable to in vivo retinal imaging.[14] As obligate hibernators, 13-LGS are used widely to study unique hypometabolic adaptations of the heart, kidney, skeletal muscle, and adipose tissue.[15] "Euthermia" describes their active physiologic state of homeothermic metabolism typical of nonhibernating mammals, while "torpor" describes the state of hypometabolic heterothermy through which they survive winter. Torpor is not continuous all winter, but is interspersed every week or so with brief euthermic periods lasting approximately 12 hours, termed "interbout arousals."[15] Despite the fact that photoreceptors are some of the most energetically demanding cells in the body, the 13-LGS retina has been studied infrequently during the torpid state. Limited work

has suggested reversibly shortened (or potentially eliminated) photoreceptor OS, depleted IS mitochondria, and remodeled ribbon synapses.[16–19] Such retinal changes provide an "experiment of nature" to probe the subcellular origin of the outer reflective signals seen with OCT retinal imaging. We leveraged the natural and reversible structural phenotypes of the torpid 13-LGS photoreceptors to better understand how this outer retinal remodeling affects OCT outer hyperreflective bands, and how these patterns compare with histologic structure.

Methods

Animal Subjects

We obtained 22 13-LGSs (*Ictidomys tridecemlineatus*; 16 female, 6 male; 5–19 months old) from the University of Wisconsin Oshkosh Squirrel Colony for use in this study at the Medical College of Wisconsin during euthermic and/or torpid physiological states (Supplementary Table S1). Euthermic 13-LGS were kept on a natural photoperiod, with light adjusted every 2 weeks to replicate ambient day lengths in Wisconsin. Starting in late summer, spontaneously torpid animals were transitioned to a dark 4°C hibernaculum; brief daily checks under red light detected any euthermic activity. Squirrel body temperature, detected by a FLIR E60 thermal imaging camera (FLIR Systems, Inc., Wilsonville, OR, USA) and/or by subcutaneous IPTT-300 temperature transponders (Bio Medic Data Systems, Seaford, DE, USA), was used to verify physiologic state (Supplementary Fig. S1). All imaging and euthanasia were performed between the hours of 10 AM and 3 PM. The experimental procedures described were approved by the Institutional Animal Care and Use Committee of the Medical College of Wisconsin (AUA00005654), and were in accordance with the ARVO Statement for the Use of Animals in Ophthalmic and Vision Research. Data were assessed for normality using the Kolmogorov-Smirnov test in InStat (GraphPad 3.1, La Jolla, CA, USA), and paired *t*-tests were used accordingly to test for statistical significance.

Optical Coherence Tomography

Euthermic 13-LGSs were anesthetized with inhaled isoflurane (5% induction, 2%–4% maintenance) in 1 L/min oxygen flow in April (normal timeframe for emergence from hibernation), June (normal timeframe for peak euthermic activity), or November (normal timeframe for hibernation). The same 13-LGSs, but in a torpid state, were removed from the hibernaculum during November, February, or March (early, middle, or late in the hibernation season) and imaged within 10 minutes after exposure to room temperature. A torpid 13-LGS takes approximately one breath per minute,[20] and consumes approximately 2% to 3% of the oxygen they inhale with 160 breaths per minute in a euthermic state.[21] Therefore, torpid animals did not require anesthesia induction, but were maintained on 0.5% to 2% isoflurane in 0.5 L/min oxygen flow solely to limit movement during ocular speculum placement and to suppress arousal to euthermia. Fourteen 13-LGSs were used for retinal imaging only, four for corneal imaging only, and four for both (Supplementary Table S1).

In preparation for OCT, one or both eyes were dilated and cyclopleged with phenylephrine hydrochloride (2.5%) and tropicamide (1%). Wetting eye drops were applied every 1 to 2 minutes throughout OCT examination. Imaging was performed with a Bioptigen Envisu R2200 Spectral Domain OCT system (Leica Microsystems, Wetzlar, Germany), equipped with a Superlum Broadlighter T870 light source centered at 878.4 nm with a 186.3 nm bandwidth (Superlum, Cork, Ireland). The Bioptigen rabbit lens was used for retinal imaging, whereas the 12-mm telecentric lens was used for corneal imaging.

Vertical line scans (650 or 1000 A-scans/B-scan; 100 repeated B-scans) of the retina were acquired at the approximated posterior pole with horizontal optic nerve and visual streak visible in each scan (Figs. 1B, 1C). A total of 20 to 50 B-scans were aligned with rigid-registration and averaged using custom software.[22] The raw images were used for analysis, and some were contrast stretched equally (18th/90th percentile gray values) in Photoshop CS6 (Adobe Systems, San Jose, CA, USA). This histogram was chosen because it did not oversaturate the euthermic images and helped visualize the features in the torpid 13-LGS retina (while keeping any disparity of signal between the two states apparent). Custom software (OCT Reflectivity Analytics) then was used to measure retinal axial layer thicknesses or distances between outer hyperreflective bands of reflectivity.[12] Nine, 5-pixel (~27.6 μm) wide longitudinal reflectance profiles (LRPs) were collected from the center of the visual streak (where the retina was thickest), then from four superior and four inferior locations with 50 μm lateral spacing between each LRP. Layer boundaries of nerve fiber layer (NFL), ganglion cell layer (GCL), inner plexiform layer (IPL), inner nuclear layer (INL), outer nuclear layer (ONL), and choroid, with local maxima of outer plexiform layer (OPL), ELM, the four outer retinal hyperreflective bands, and the hyperreflective junction of the inner choroid (that separates the choriocapillaris from the rest of the choroid) were selected and averaged over the nine LRP sampling locations for layer thickness and peak-to-peak measurements. Corneal volume scans (1000 A-scans/B-scan; 100 B-scans) were acquired, and corneal layer thicknesses were measured from a single B-scan at the approximate central cornea with the Bioptigen InVivoVue 2.4 software (Leica Microsystems).

We used the following Band 1-4 (B1-4) assignments for the outer retinal bands: B1 as the anatomic ELM, B2 as either the EZ or IS/OS junction, B3 as the IZ or outer segment tips (OST), and B4 as RPE-basal lamina-Bruch's membrane[23] (Fig. 1D).

Histology and Microscopy

Six 13-LGSs were imaged with OCT, then subsequently used for histologic analysis. These 13-LGSs were euthanized by decapitation in November: three euthermic (under isoflurane anesthesia) and three torpid (without anesthesia) animals. One eye was enucleated and the whole globe was immersion-fixed overnight in 2% paraformaldehyde, 2% glutaraldehyde in 0.1 M cacodylate buffer at 4°C. This whole globe fixation method (without puncture) was chosen due to its success in preserving the IS/OS interface in a recent ultrastructural study.[24] Following fixation, the cornea and lens were removed, and eye cups were postfixed in 1% osmium tetroxide followed by dehydration in a graded methanol series. Subsequently, eye cups were infused with acetonitrile before infiltration with Embed 812 (EMS, Hatfield, PA, USA). Then, 0.5 μm sections were cut on an Ultracut E microtome (Reichert-Jung/Leica Microsystems) and stained with 1% toluidine blue for light microscopy (LM).

Contralateral eyes from the six 13-LGSs euthanized for LM histology after OCT were used for immunocytochemistry. These eyes were immersion-fixed for 10 minutes using 4% paraformaldehyde in PBS (pH, 7.4). Following fixation, cryosection immunocytochemistry was performed as described previously.[14] Primary antibodies and probes used were: anti-cytochrome oxidase (labels mitochondria, 1:100, A-6403; Molecular Probes, Eugene, OR, USA), anti-L/M opsin (labels M-cone OS, 1:500, AB3272; EMD Millipore, Burlington, MA, USA), and peanut agglutinin (labels cone sheaths, 1:100, B-

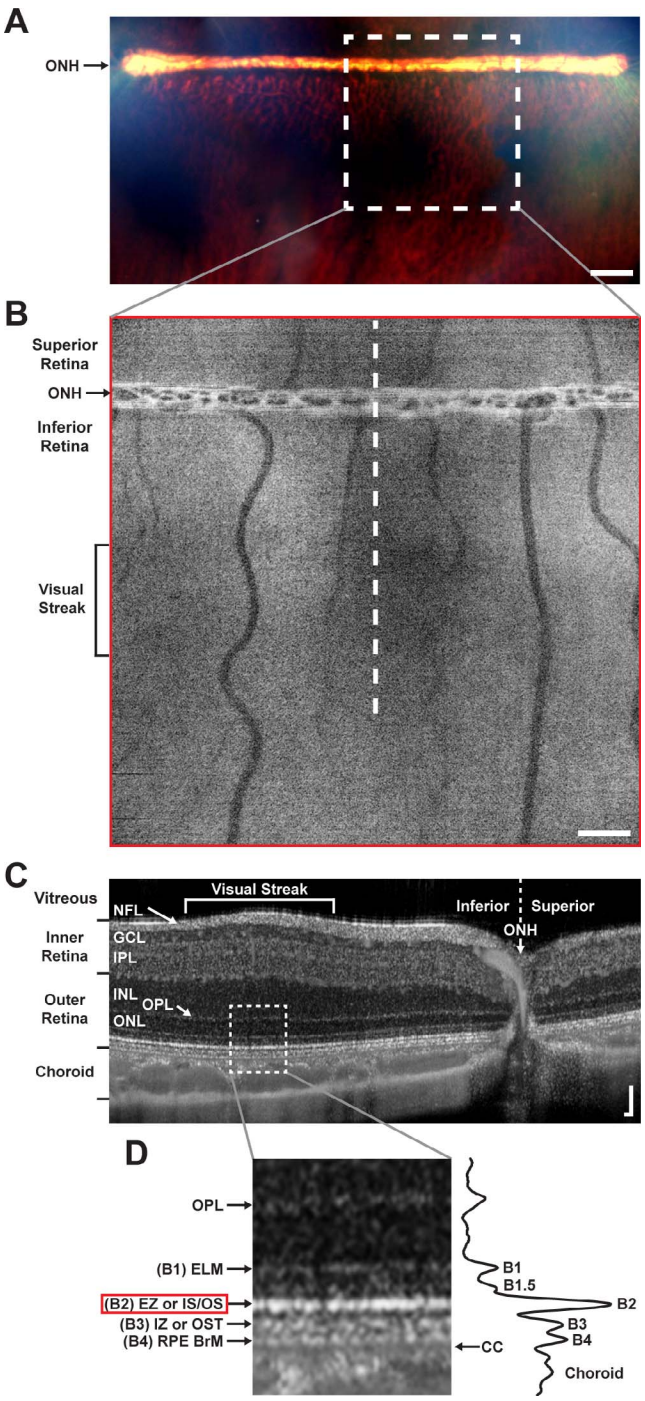

Figure 1. Example of OCT imaging in a euthermic 13-LGS. (**A**) Fundus montage taken with a Phoenix Micron III camera (Phoenix Research Labs, Pleasanton, CA, USA), including the horizontal optic nerve head (ONH). *Dashed-line box* indicates position of (**B**). *Scale bar*: 500 μm. (**B**) En face volumetric projection of band 2 signal, *dashed line* indicates vertical b-scan region shown in (**C**). *Scale bar*: 200 μm. (**C**) 13-LGS retinal layers visualized with OCT, including the visual streak. *Dashed-line box* indicates area enlarged in (**D**). *Scale bars*: 50 μm. (**D**) 13-LGS outer retinal layers, with outer band assignment hypotheses on the *left* and an LRP of the displayed region, including our proposed B1-4 assignments on the *right*. RPE BrM, RPE-basal lamina-Bruch's membrane; CC, choriocapillaris. This animal was not otherwise used for this study. Images in panels **A**–**D** were contrast stretched for display purposes.

1075; Vector Laboratories, Inc., Burlingame, CA, USA). Primary antibodies and probes were diluted in PBS containing 0.5% bovine serum albumin and 0.1% Triton X-100 (PBTA), in which tissue sections were incubated overnight at 4°C. Then, 100 μm sections were rinsed 1 × 1 hour and 5 × 5 minutes using PBTA and then incubated in a cocktail of corresponding secondary fluorophores overnight at 4°C (1:200; Jackson ImmunoResearch, Inc., West Grove, PA, USA). After rinsing and mounting, sections were imaged using an Olympus Fluoview 1000 laser scanning confocal microscope (Olympus, Inc., Center Valley, PA, USA) for immunofluorescence (IF) analysis.

All histology images used for analysis were from the 13-LGS inferior retina (approximately the visual streak), at the posterior pole. Inner segment myoid (ISm), inner segment ellipsoid (ISe), OS, and RPE distances were measured manually in ImageJ[25] and averaged from nine cone photoreceptors from each retina. All cones used in the analysis were verified to be vertically oriented by making sure inner and outer segments of the same cell were in the viewing plane.

For transmission electron microscopy (TEM), 70 nm sections were cut using a PowerTome MT-XL ultramicrotome (RMC Boeckeler, Tucson, AZ, USA), collected onto 200 mesh hexagonal grids (EMS, Hatfield, PA, USA), and stained with lead citrate and uranyl acetate. Imaging was performed on a H-600 transmission electron microscope (Hitachi, Krefeld, Germany).

Results

13-LGS Retinal OCT During Euthermia and Torpor

OCT images acquired from the same animal revealed qualitative and quantitative torpor-induced changes relative to the same retina in a euthermic state (Fig. 2). Four outer hyperreflective bands were detected in 100% (18/18) of euthermic and 87% (13/15) of torpid eyes imaged. Between B1 and B2, an additional local maximum of unknown origin (herein referred to as reflective band "B1.5") was detected in 100% (18/18) of euthermic, but only 13% (2/15) of torpid eyes (e.g., DM_150604 in Fig. 2). Intra-animal OCT retinal layer thickness and outer band local maxima peak-to-peak distance data were obtained and quantified (Fig. 3, Supplementary Table S2). In some instances in torpid retinas, local maxima for the OPL and/or B1 were undetectable, or neighboring outer bands were indistinguishable from each other (asterisks, Supplementary Table S2); these 13-LGSs were removed from the relevant grouped analysis.

As shown in Figure 3, the only inner retinal layer to show a significant difference in thickness between euthermic and torpid states was the INL (euthermic = 81.90 ± 4.07 vs. torpid = 85.76 ± 4.44 μm; $P = 0.041$, paired *t*-test; Fig. 3A). In contrast, all outer retinal layers showed significant differences in thickness between euthermic and torpid states. While the ONL thickness, B1-B2 distance, and B3-B4 distance all were increased in the torpid state relative to the euthermic state, the B2-B3 distance, choriocapillaris thickness, and choroid thickness all were decreased in the torpid state relative to the euthermic state (Figs. 3B, 3C; Supplementary Table S2).

Torpor-Induced Edema of the Corneal Stroma

The eyes of all torpid animals exhibited pallor compared to euthermic subjects, which is best described as an abnormal bluish-gray hue (Supplementary Fig. S2) suggesting an ocular media opacity. The location of the opacity (i.e., cornea or lens), in addition to pupil dilation, was impossible to confirm by the naked eye. To investigate this phenomenon, we looked to the anterior segment for possible changes affecting imaging light

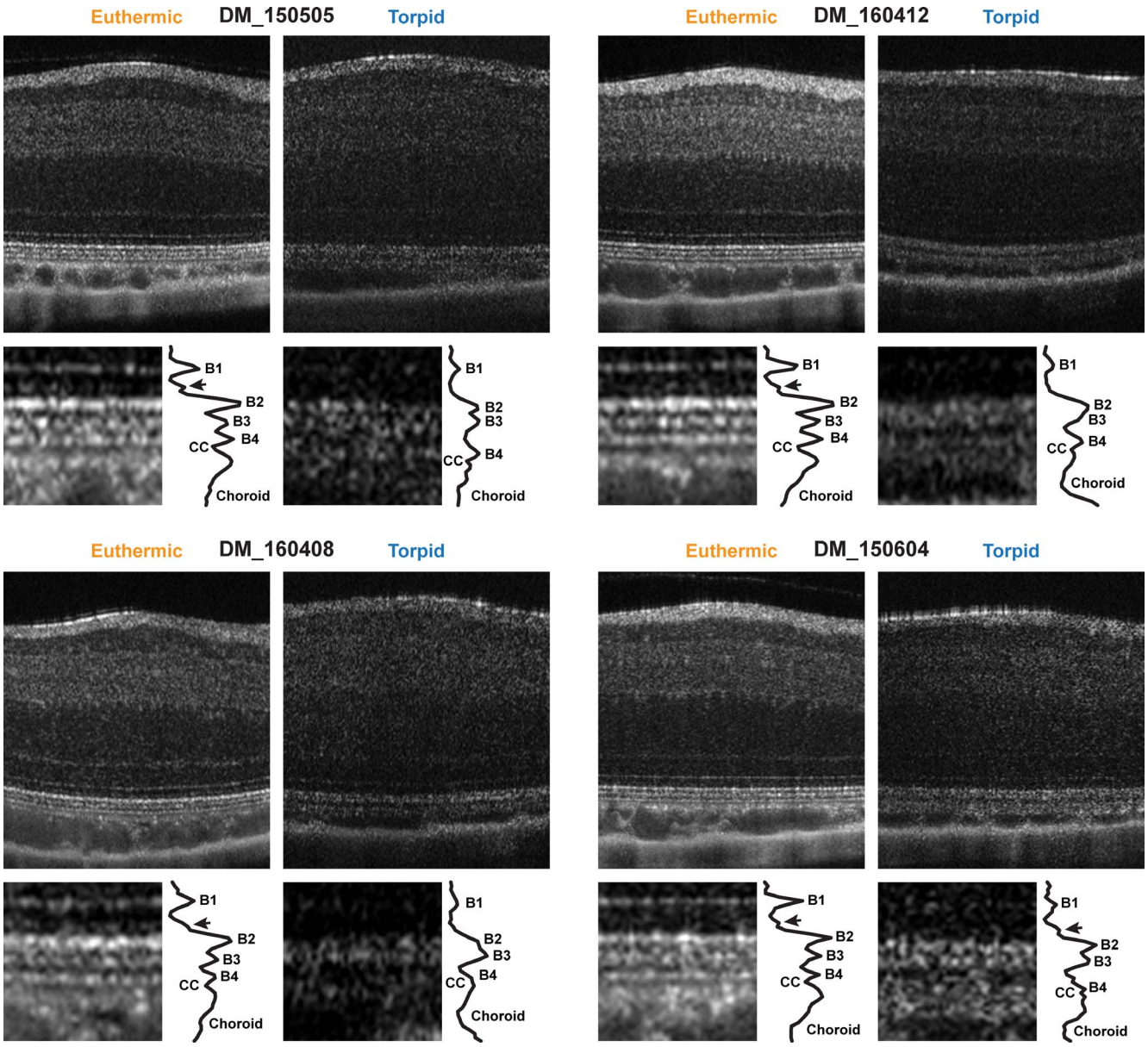

Figure 2. Intra-animal comparisons of euthermic and torpid 13-LGS retinas. *Insets* are close-up images of the outer retina at the visual streak, with corresponding LRP. An additional outer band was detected between B1 and B2 (*arrows*) in all euthermic 13-LGS (12/12), but only 1/12 of the same retinas in torpor (DM_150604) in these comparisons. Images were contrast stretched for display purposes.

delivery and capture. Subsequent intra-animal corneal OCT imaging in euthermic and torpid states revealed no torpor-induced change in epithelial layer thickness (51.75 ± 6.16 [euthermic] vs. 53.46 ± 4.62 [torpid] μm; $n = 8$, $P = 0.57$, paired *t*-test), but significantly increased torpid stroma thickness relative to euthermic state stroma (226.75 ± 37.61 [torpid] vs. 120.13 ± 7.86 [euthermic] μm, $n = 8$, $P = <0.0001$, paired *t*-test; Fig. 4), a phenomenon that appears to have been missed with hematoxylin and eosin (H&E) histology.[26]

Intra-Animal OCT and Histological Comparison in Euthermic and Torpid 13-LGS Retina

To examine how the four hyperreflective bands in the outer retina compared to histology, we quantified the distances between OCT local maxima of the four hyperreflective bands and then the histologic distances of photoreceptor structure visualized in light micrographs and immunofluorescence images (Fig. 5; Supplementary Tables S3, S4). Euthermic OCTs collected from both eyes of the same animal showed bilateral symmetry of the distances between B1 and B2, B2 and B3, and B3 and B4 (Supplementary Fig. S3). On average, shorter ISe were seen when comparing torpid to euthermic retina light micrographs, taking up 33% ± 2% ($n = 3$) and 47% ± 3% ($n = 3$) of the total IS in torpid and euthermic retinas, respectively (Supplementary Table S3). Torpid OS seen with LM did not have the uniform and orderly morphology seen in euthermic photoreceptors (red arrows, Fig. 6). Additionally, a marked gap between ISe and OS was visible in several torpid photoreceptors examined with LM (yellow arrows, Fig. 6), suggesting a movement and/or

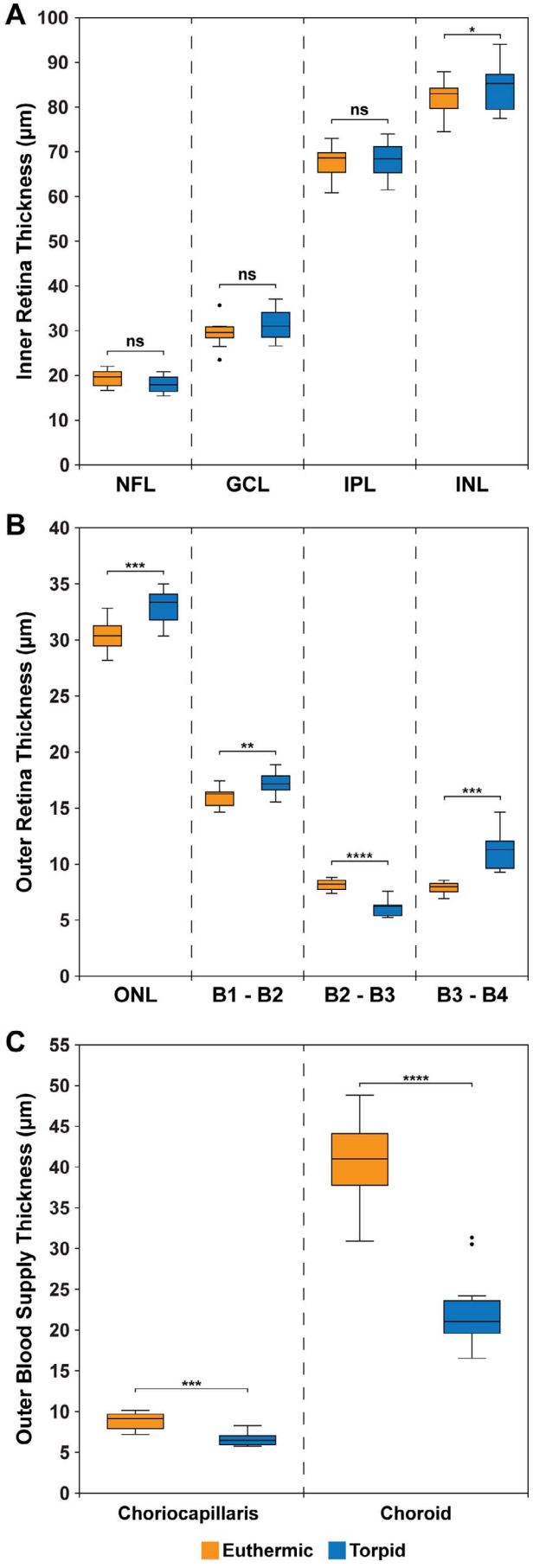

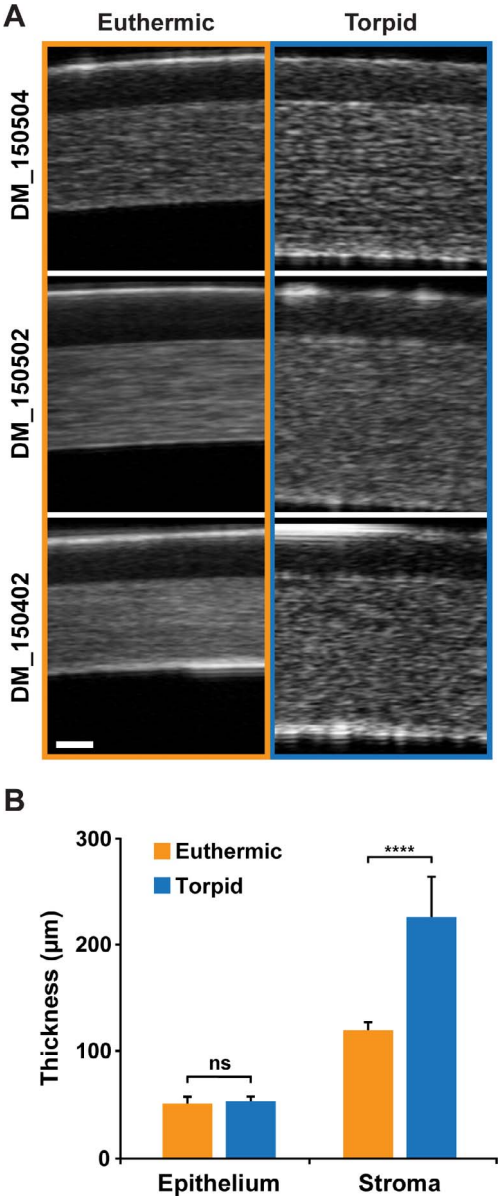

FIGURE 4. Intra-animal comparisons of euthermic and torpid 13-LGS corneas. (**A**) Three examples of comparative corneal OCT images. (**B**) Epithelial layer thickness was similar in both physiological states, but the stroma was significantly thicker ($p < 0.0001$, $n = 8$, paired *t*-test). *Scale bar*: 50 µm. Images were contrast stretched for display purposes.

elimination of mitochondria in this area. The punctate photoreceptor nuclear staining in the torpid retina suggests increased heterochromatin (white arrows, Fig. 6). Despite the disorganization seen in the torpid retina, immunofluorescent staining for anti-cytochrome oxidase, L/M-opsin, and peanut agglutinin looked similar in euthermic and torpid photoreceptors (Figs. 5A, 5B).

FIGURE 3. Box-and-whisker plots of inner retina (**A**), outer retina (**B**), and outer blood supply (**C**) thickness in axial depth of euthermic (*orange*) and torpid (*blue*) retinas. Boxes show median and interquartile ranges, *whiskers* show maximum and minimum values, and *circles* show outliers. Not significant (ns) = $P > 0.05$; $^{*}P < 0.05$; $^{**}P < 0.01$; $^{***}P < 0.001$; $^{****}P < 0.0001$, paired *t*-test.

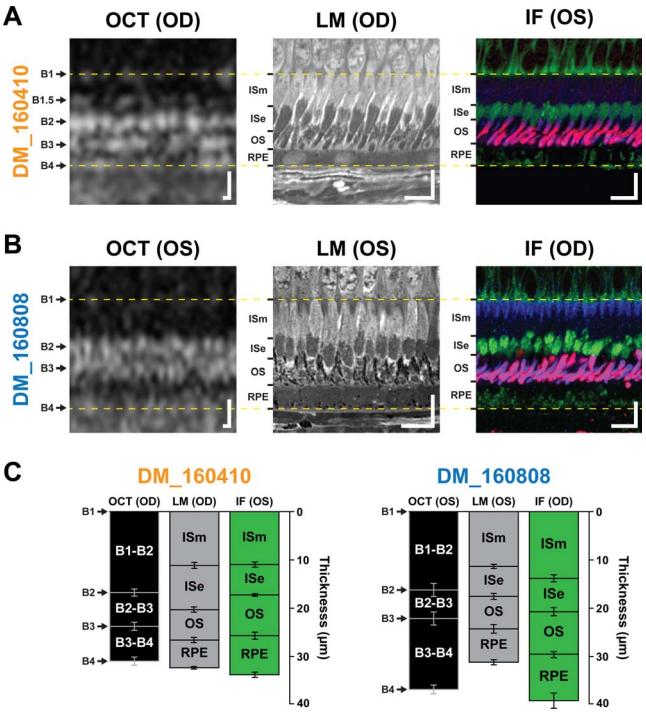

Figure 5. Intra-animal comparisons of euthermic (*orange text*; [**A**]) and torpid (*blue text*; [**B**]) 13-LGS retinal visual streak using in vivo OCT and ex vivo LM (stained with toluidine blue) and IF (*green*, anti-cytochrome oxidase; *blue*, anti-peanut agglutinin; *red*, anti-L/M-opsin). LM and IF images in (**A**) and (**B**) were scaled to the OCT such that B1 aligns the ELM and B4 aligns with the RPE BrM (*yellow dashed lines*). While these images appear similar in scale, there is a 5% to 20% difference in axial scale that was required for this alignment. *Scale bars*: 10 μm. The euthermic and torpid *bar graphs* provide mixed results regarding the subcellular origin of B2 (**C**). This band most often aligned to the ISe, supporting the EZ nomenclature for B2; however, the euthermic OCT to IF data in this representative comparison nicely aligns with the IS/OS junction. While we demonstrated bilateral symmetry of peak-to-peak measurements in euthermic 13-LGS OCT (Supplementary Fig. S3), it is important to note that the IF data here are from the opposite eye relative to the OCT image and bar graphs. OS next to the method refers to the left eye, while OS on the bar graphs refer to outer segment axial distance. OCT images were contrast stretched for display purposes.

Electron Microscopy of Euthermic and Torpid 13-LGS Cones

We next used TEM to further investigate the disorganization of cone structures during the torpid state in more detail at the ultrastructural level. The ISe of torpid photoreceptors contained a cytoplasmic region basal to the OS that lacked the high concentration of mitochondria seen in euthermic photoreceptors (Figs. 7A, 7B). On average, this gap from the IS mitochondria to the distal IS membrane was 2.5 μm (range, 1.6–5.7 μm; $n = 9$ cones). There was even evidence of absent mitochondria and mitochondrial degeneration in some of the ISe examined (Supplementary Figs. S4B, S4C).

Also striking were the highly disrupted cone OS discs (Fig. 7) that appeared to pull away from the cone sheath, as has been observed previously.[16] This was never observed in cones of euthermic animals, suggesting that the OS disc disruption was not due to a fixation artifact. In fact, of the shortened discs that remained in the torpid OS, the morphology was remarkably well preserved, particularly the disc rims and open discs continuous with the OS plasma membrane, further suggesting that the phenotype is not artifactual. However, our data did not rule out the possibility that while in vivo OSs may be morphologically intact in a torpid animal, they are substantially more sensitive to variable disruption during fixation. Oftentimes, only the OS discs appeared to be extremely extended and dysmorphic (Supplementary Fig. S4A). In addition, while not thoroughly assessed in this study, the RPE appears similar in these two states. Melanosome-rich apical processes extend just anterior to the distal IS membrane in both states (Figs. 7G, 7H).

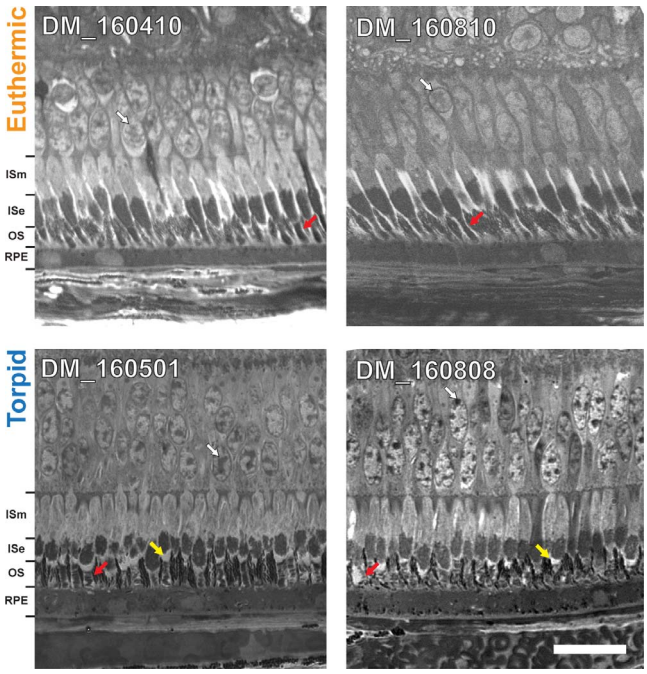

Figure 6. Light micrographs (stained with 1% toluidine blue) of euthermic and torpid 13-LGS photoreceptors. The chromatin in the micrographs of torpid 13-LGS photoreceptors appeared more densely packed and stained darker with toluidine blue (*white arrows*). OS appears uniform in euthermic LM samples (*red arrows*, *top row*), but disrupted in the torpid LM samples (*red arrows*, *bottom row*). A gap that forms between IS and OS of the torpid 13-LGS photoreceptors is visible at this scale (*yellow arrows*). *Scale bar*: 50 μm.

Discussion

Hibernation provides a model of drastic metabolic inhibition in which to study reversible retinal remodeling. To our knowledge, we provided the first in vivo cross-sectional assessment of a mammalian retina in two naturally-occurring physiologic states: euthermia and torpor. We observed significant ONL thickening in torpid 13-LGSs. While the basis of this ONL thickening is not known, it may be related to changes in the Müller glia and a retinal glymphatic system, which have been proposed to cause INL thickening in multiple sclerosis.[27] Alternatively, photoreceptor stress is thought to cause ONL thickening with normal aging,[28] and preceding cell loss in patients with age-related macular degeneration (AMD).[29,30] It is unclear whether there is any connection between ONL thickening during torpor, and that which occurs in humans as a result of ageing and retinal disease. Hibernating mammals have adapted protective mechanisms to prevent cell loss during torpor,[31] but these protective mechanisms have not been studied in the retina. It is possible that protective growth factors that respond to retinal insult (e.g., fibroblast growth factor,[32] and/or ciliary neurotrophic factor[33]) have similar roles in protecting against cell loss during torpor, which might result

Investigative Ophthalmology & Visual Science

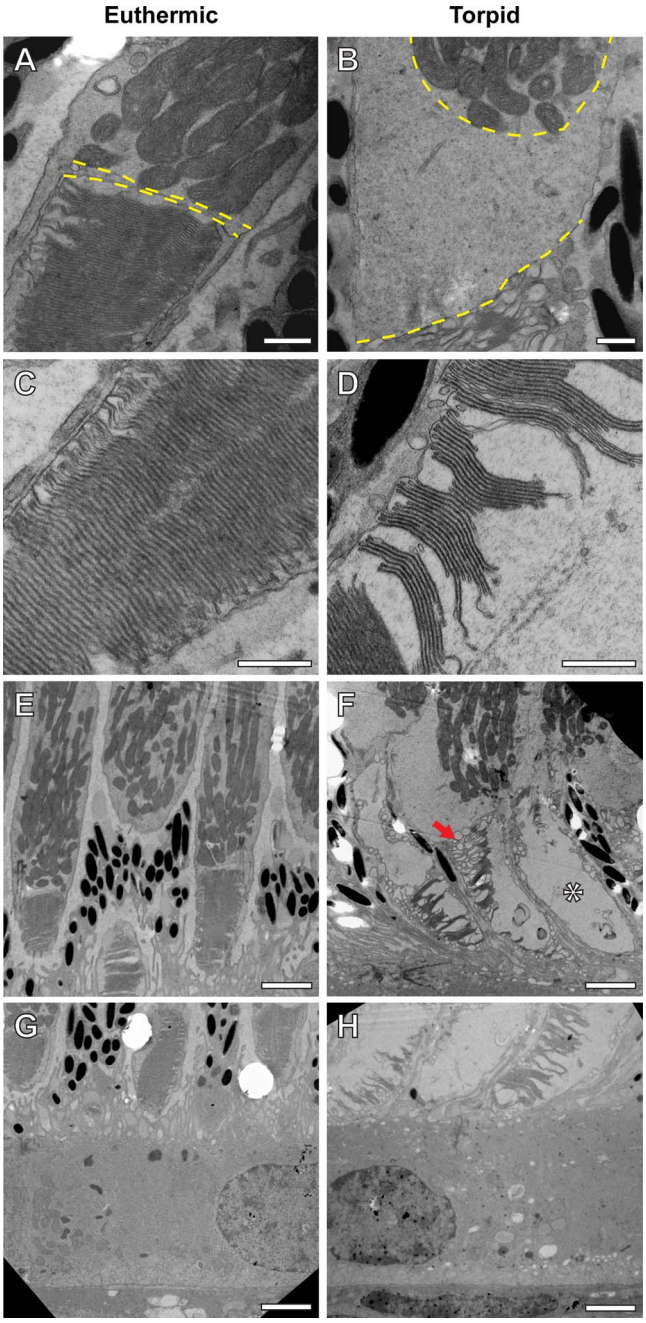

FIGURE 7. TEM images of euthermic (DM_160410) and torpid (DM_160808) 13-LGS IS/OS ([**A**, **B**]; *scale bars*: 500 nm) and the distal IS gap (boundaries highlighted by *yellow dashed line*), cone disc packing ([**C**, **D**]; *scale bars*: 500 nm), and a lower magnification view of cone photoreceptors (*red arrow*, vesiculation of OS; *asterisk*, cone sheath with nearly absent OS) and RPE ([**E**–**H**]; *scale bars*: 2 μm).

in cellular enlargement and a corresponding increase in ONL thickness.

The choriocapillaris and choroid were significantly thinner during torpor, the natural hypoxic state to which squirrels are demonstrably tolerant.[34] Choroidal thinning has been visualized with OCT in disorders with pathologic hypoxic implications, such as pseudoexfoliation syndrome[35] and Alzheimer's disease,[36] but it remains unclear if any parallels can be found with a normal torpid state. Our data regarding choroidal thinning in torpor are limited in that the measurements were taken only at the visual streak. A choroidal segmentation approach[37] or OCT-angiography would more robustly describe this phenomenon across the retina.

The poor image quality observed while imaging torpid 13-LGSs with OCT can now be explained partly by corneal stromal thickening that is missed by conventional histologic approaches.[26] Our results indicated a 2-fold increase in stromal thickness during torpor, resembling mild endothelial dystrophies (Supplementary Fig. S2).[38,39] Corneal swelling by stromal edema has been documented using OCT in cold and hypoxic human corneas,[40–43] possibly due to decreased metabolic Na/K ATPase pump activity within the corneal endothelium.[44] It is likely that endothelial cell death is avoided in hibernation, allowing for fast reversal of this stromal edema in room temperature normoxia. The 13-LGS had presumably evolved ways to avoid corneal and lens damage throughout hibernation, as vision becomes an immediate priority when emerging from hibernation in spring. While retinal structural recovery takes hours to days to fully recover after euthermia is first regained,[16] imaging under isoflurane anesthesia at room temperature while applying frequent eye drops seems to provide an appropriate balance of suppressing arousal to euthermia while improving optical clarity for our retinal imaging purposes.

The subcellular origin of the outer hyperreflective bands, namely B2 and B3, is controversial,[3,5] but is critically important to validate, since metrics, such as EZ width, are being used as outcome measures in clinical trials.[10,11] Using a cone-dominant species offers a novel contribution toward this debate, but further work correlating OCT with histology is warranted. Using electron microscopy, Remé and Young[16] described three key photoreceptor changes in the 13-LGS that pertain to hypotheses of B2 and B3 hyperreflective band origin. (1) With transverse sections of IS ellipsoids from "active" (assuming euthermic) and "hibernating" (assuming torpid), they described 13-LGS mitochondria as reduced in size and number during hibernation.[16] However, more recent 3-dimensional (3D) photoreceptor reconstructions show instead that, while individual mitochondrial volumes are reduced and their packing is rearranged, their numbers actually increase during torpor (Kaden T, et al. *IOVS* 2013;54:ARVO E-Abstract 6082). Our LM data support a decrease in mitochondrial (ISe) length in the torpid retina, but more work is needed to look at mitochondrial structure throughout the hibernation cycle. (2) During torpor, mitochondria migrated away from the connecting cilium and any anatomical "IS/OS junction," creating a void between the IS mitochondria and the distal IS membrane. While simulations suggest that this torpor-induced mitochondrial remodeling changes how light is focused onto cone photoreceptors (Li W, et al. *IOVS* 2017;58:ARVO E-Abstract 1037), it is not clear how these changes translate to the OCT image. (3) Hibernating OS discs often were narrower within the cone sheath, while the whole OS was shortened or eliminated altogether. While it is difficult to obtain exact measurements of the complete disorganized OS structure during torpor with these 2D TEM images, our EM analysis shows that the cone sheath remains intact, but the few persisting OS discs within are retracted from the sheath (Fig. 7). While cone disruption was seen in all torpid cones we examined, the changes to inner and outer segments are highly variable.

Our intra-animal OCT comparisons revealed several changes in the outer hyperreflective bands that corresponded to the photoreceptors and RPE. The averaged distance from B1 to B2 increased slightly during torpor (17.2 μm) compared to during euthermia (15.9 μm), and both fell short of the IS length observed previously by histology (20.1 μm).[16] Our averaged B2 to B3 OCT measurements also compared well to the

"summertime control" 13-LGS OS length results reported by Remé and Young[16] (8.1 vs. 7.4 μm, respectively), and this distance, indeed, decreased in torpor (our study = 6.0 μm, reported as "shorter" in Remé and Young[16]). Taking these intra-animal OCT comparisons together with our OCT to LM analysis, the 13-LGS B2 aligns to the outer one-third of the anatomical IS ellipsoid, which supports the model that mitochondria is a source of reflection in the IS.[45,46] However, when comparing the OCT to IF axial measurements, the B1 to B2 distance compared well to the total IS distance, which supported the IS/OS theory for B2 (Supplementary Table S4).[5] The limitations of using these IF sets for structural comparisons are that antibody labeling of inner segment COX is being analyzed, rather than the IS structure itself (as in LM). The disconnect between OCT and histologic measurements is well documented in other species,[47–50] and our results highlighted an instance where the B1 to B2 measurements were consistent across 13-LGSs (euthermic = 15.9 ± 0.9 μm, torpid = 17.2 ± 0.9 μm; Supplementary Table S2) and bilaterally in the same 13-LGSs (Supplementary Fig. S3), yet different tissue preparations and microscopy techniques revealed conflicting answers to the subcellular origin of Band 2 (Supplementary Tables S3, S4). While these OCT to LM or IF comparisons were done using the same animal, a limitation in this analysis is that only a single inferior retinal location was analyzed. It is possible that the outer hyperreflective bands and photoreceptor structures vary in axial distance across inferior and superior retinal locations. A more comprehensive histologic comparison, one that includes several eccentricities relative to the optic nerve head (ONH) is warranted, ideally comparing identical retinal locations in vivo and ex vivo.

A potential limitation arises with the sex of 13-LGSs being skewed toward females in this study. While differences between the sexes are not expected with the outer retinal axial measurements, we cannot rule out hormonal difference affecting these data. Males are known to emerge from hibernation 2 weeks before females for example,[51] a practice continued in the captive colony, and this may affect the degree of torpor-induced changes they experience each year.

In torpid retinas, OS discs often are separated into clumps or tilted, so volumetric OS quantification with scanning electron microscopy would likely provide a more complete depiction of torpid OS changes. It recently has been reported that OS disc morphogenesis occurs through a peripherin-dependent inhibition of ectosome release from the OS cilia.[52] Due to decreased cellular metabolism during hibernation, it is possible that an insufficient concentration of peripherin is synthesized and transported to the OS, leading to the observed accumulation of ciliary ectosomes in the interphotoreceptor space. Another explanation for the mixed state of disorganized OS and fully formed discs could originate from the interbout arousals that occur during hibernation. It is possible that the squirrel's return to euthermia for approximately 12 hours permit brief periods of morphologically-normal OS disc formation. However, some cone outer segments are completely absent (Fig. 7F), as previously reported by Kuwabara.[17] The most striking change to the outer OCT bands was a significant increase in the distance between B3 and B4 (on average, 7.7 μm in euthermia, versus 11.3 μm in torpor). This increase is peculiar in that it was not detectable with our direct ex vivo comparisons. It is possible that the lipid deposits and "regular whorls" (as described by Remé and Young[16]) of tubules that build up in the torpid RPE contribute to this gap formation, and that this distance is decreased during histologic processing. However, our IF RPE measurements ranged from 2.1 to 3.0 μm larger than the contralateral LM RPE measurements, which suggests that the fixation method alone altered our results for this comparison. Fixation artifacts appeared to be limited in euthermic retinas, with B1 to B4 distances comparing well to ELM to BrM lengths. More OCT-to-histology comparisons of these fine structures should be done relative to different fixation protocols, as has been done in the cone-dominant tree shrew.[48] This study is limited in that is does not thoroughly assess RPE apical processes and their melanosomes, which are known reflectors related to these posterior reflective bands.[53,54] However, initial observations suggest that these RPE apical processes appear normal in torpid animals.

Most studies using hibernating animals compare only the most extreme hibernation phenotypes, and ours is no exception. While the variability in OS, ISe, and RPE changes does not seem to be related to the duration of hibernation,[16] it is likely due to the temporal scale relative to interbout arousals (to euthermia) throughout the hibernation season.[15] This source of physiologic variability should be accounted for when analyzing these natural phenomena to develop a more comprehensive understanding of circannual structural changes. In addition, the axial resolution of the OCT used in this study is approximately 1.35 μm,[55,56] suitable for detection of these fine changes in band-to-band distances. However, it is difficult to control for any refractive changes that occur to the biological structures being imaged during torpor. While not directly tested in this study, it is possible that the increased corneal thickness changes the light scattering properties being collected with OCT. A better understanding is needed regarding the specific refractive indices of each retinal structure in vivo, how they can change with corneal thickening, and how they relate to OCT signal scaling when comparing axial distances.

Remodeling of the 13-LGS retina during hibernation presents a unique opportunity to further understand the subcellular basis of photoreceptor reflectance in noninvasive retinal imagery. The variability of human outer band measurements[12,53] alongside limited human histology justifies continued in vivo to ex vivo comparative analyses in animal models. While AO-OCT provides the highest resolution yet toward revealing the origin of these signals,[57] direct comparisons of AO-OCT to histology of the same retinal locations are lacking. A multimodal, intra-animal approach using AO-OCT, OCT, with LM and EM at the same retinal location with limited fixation artifact is feasible and presents a logical direction toward resolving the hyperreflective band controversy.

Acknowledgments

The authors thank Christine Skumatz, Kenneth Allen, and Eric Jensen for their contributions to 13-LGS care and IACUC protocol development, Wei Li and Alex Salmon for valuable discussion regarding the OCT results, and Joseph Besharse for valuable discussion regarding the EM results.

Supported by The Catherine and Walter Lindsay Fund of the Greater Milwaukee Foundation (MCW), Foundation Fighting Blindness consortium PPA-0617-0718-UCSF (MCW), the Alcon Research Institute (MCW), an Unrestricted Grant from the Research to Prevent Blindness (CC), and the National Science Foundation IIS-0808772 and ITR-0331697 (UCSB). Research reported in this publication was supported by the National Eye Institute of the National Institutes of Health (NIH, Bethesda, MD, USA) under award numbers P30EY001931 and T32EY014537. This investigation was conducted in a facility constructed with support from Research Facilities Improvement Program Grant Number C06RR016511 from the National Center for Research Resources, NIH. The authors alone are responsible for the content and writing of this paper.

Disclosure: **B.S. Sajdak**, None; **B.A. Bell**, None; **T.R. Lewis**, None; **G. Luna**, None; **G.S. Cornwell**, None; **S.K. Fisher**, None; **D.K. Merriman**, None; **J. Carroll**, None

References

1. Huang D, Swanson EA, Lin CP, et al. Optical coherence tomography. *Science*. 1991;254:1178–1181.
2. Fujimoto J, Swanson E. The development, commercialization, and impact of optical coherence tomography. *Invest Ophthalmol Vis Sci*. 2016;57:OCT1–OCT13.
3. Staurenghi G, Sadda S, Chakravarthy U, Spaide RF, Panel IO. Proposed lexicon for anatomic landmarks in normal posterior segment spectral-domain optical coherence tomography: the IN•OCT consensus. *Ophthalmology*. 2014;121:1572–1578.
4. Spaide RF, Curcio CA. Anatomical correlates to the bands seen in the outer retina by optical coherence tomography: literature review and model. *Retina*. 2011;31:1609–1619.
5. Jonnal RS, Kocaoglu OP, Zawadzki RJ, Lee SH, Werner JS, Miller DT. The cellular origins of the outer retinal bands in optical coherence tomography images. *Invest Ophthalmol Vis Sci*. 2014;55:7904–7918.
6. Jonnal RS, Gorczynska I, Migacz JV, Azimipour M, Zawadzki RJ, Werner JS. The properties of outer retinal band three investigated with adaptive-optics optical coherence tomography. *Invest Ophthalmol Vis Sci*. 2017;58:4559–4568.
7. Flatter JA, Cooper RF, Dubow MJ, et al. Outer retinal structure after closed-globe blunt ocular trauma. *Retina*. 2014;34:2133–2146.
8. Langlo CS, Patterson EJ, Higgins BP, et al. Residual foveal cone structure in *CNGB3*-associated achromatopsia. *Invest Ophthalmol Vis Sci*. 2016;57:3984–3995.
9. Scoles D, Flatter JA, Cooper RF, et al. Assessing photoreceptor structure associated with ellipsoid zone disruptions visualized with optical coherence tomography. *Retina*. 2016;36:91–103.
10. Hariri AH, Velaga SB, Girach A, et al. Measurement and reproducibility of preserved ellipsoid zone area and preserved retinal pigment epithelium area in eyes with choroideremia. *Am J Ophthalmol*. 2017;179:110–117.
11. Smith TB, Parker M, Steinkamp PN, et al. Structure-function modeling of optical coherence tomography and standard automated perimetry in the retina of patients with autosomal dominant retinitis pigmentosa. *PLoS One*. 2016;11:e0148022.
12. Wilk MA, Wilk BM, Langlo CS, Cooper RF, Carroll J. Evaluating outer segment length as a surrogate measure of peak foveal cone density. *Vision Res*. 2017;130:57–66.
13. Curcio CA, Sloan KR, Kalina RE, Hendrickson AE. Human photoreceptor topography. *J Comp Neurol*. 1990;292:497–523.
14. Sajdak B, Sulai YN, Langlo CS, et al. Noninvasive imaging of the thirteen-lined ground squirrel photoreceptor mosaic. *Vis Neurosci*. 2016;33:e003.
15. Staples JF. Metabolic flexibility: hibernation, torpor, and estivation. *Compr Physiol*. 2016;6:737–771.
16. Remé CE, Young RW. The effects of hibernation on cone visual cells in the ground squirrel. *Invest Ophthalmol Vis Sci*. 1977;16:815–840.
17. Kuwabara T. Cytologic changes of the retina and pigment epithelium during hibernation. *Invest Ophthalmol*. 1975;14:457–467.
18. Mehta B, Snellman J, Chen S, Li W, Zenisek D. Synaptic ribbons influence the size and frequency of miniature-like evoked postsynaptic currents. *Neuron*. 2013;77:516–527.
19. Merriman DK, Sajdak BS, Li W, Jones BW. Seasonal and post-trauma remodeling in cone-dominant ground squirrel retina. *Exp Eye Res*. 2016;150:90–105.
20. Landau BR, Dawe AR. Respiration in the hibernation of the 13-lined ground squirrel. *Am J Physiol*. 1958;194:75–82.
21. Cooper ST, Sell SS, Fahrenkrog M, et al. Effects of hibernation on bone marrow transcriptome in thirteen-lined ground squirrels. *Physiol Genomics*. 2016;48:513–525.
22. Dubra A, Harvey Z. Registration of 2D images from fast scanning ophthalmic instruments. In: Fischer B, Dawant B, Lorenz C, eds. *Biomedical Image Registration*. Berlin: Springer-Verlag; 2010:60–71.
23. Tan ACS, Astroz P, Dansingani KK, et al. The evolution of the plateau, an optical coherence tomography signature seen in geographic atrophy. *Invest Ophthalmol Vis Sci*. 2017;58:2349–2358.
24. Burgoyne T, Meschede IP, Burden JJ, Bailly M, Seabra MC, Futter CE. Rod disc renewal occurs by evagination of the ciliary plasma membrane that makes cadherin-based contacts with the inner segment. *Proc Natl Acad Sci USA*. 2015;112:15922–15927.
25. Schindelin J, Arganda-Carreras I, Frise E, et al. Fiji: An open-source platform for biological-image analysis. *Nat Methods*. 2012;9:676–682.
26. Rodriguez-Ramos Fernandez J, Dubielzig RR. Ocular comparative anatomy of the family Rodentia. *Vet Ophthalmol*. 2013;16:94–99.
27. Petzold A. Retinal glymphatic system: an explanation for transient retinal layer volume changes. *Brain*. 2016;138:2816–2819.
28. Chui TY, Song H, Clark CA, Papay JA, Burns SA, Elsner AE. Cone photoreceptor packing density and the outer nuclear layer thickness in healthy subjects. *Invest Ophthalmol Vis Sci*. 2012;53:3545–3553.
29. Schmitz-Valckenberg S, Fleckenstein M, Helb HM, Charbel Issa P, Scholl HP, Holz FG. In vivo imaging of foveal sparing in geographic atrophy secondary to age-related macular degeneration. *Invest Ophthalmol Vis Sci*. 2009;50:3915–3921.
30. Sadigh S, Cideciyan AV, Sumaroka A, et al. Abnormal thickening as well as thinning of the photoreceptor layer in intermediate age-related macular degeneration. *Invest Ophthalmol Vis Sci*. 2013;54:1603–1612.
31. Carey HV, Andrews MT, Martin SL. Mammalian hibernation: cellular and molecular responses to depressed metabolism and low temperature. *Physiol Rev*. 2003;83:1153–1181.
32. Faktorovich EG, Steinberg RH, Yasumura D, Matthes MT, LaVail MM. Photoreceptor degeneration in inherited retinal dystrophy delayed by basic fibroblast growth factor. *Nature*. 1990;347:83–86.
33. Wen R, Song Y, Cheng T, et al. Injury-induced upregulation of bFGF and CNTF mRNAS in the rat retina. *J Neurosci*. 1995;15:7377–7385.
34. Larson J, Drew KL, Folkow LP, Milton SL, Park TJ. No oxygen? No problem! Intrinsic brain tolerance to hypoxia in vertebrates. *J Exp Biol*. 2014;217:1024–1039.
35. Eroglu FC, Asena L, Simsek C, Kal A, Yılmaz G. Evaluation of choroidal thickness using enhanced depth imaging by spectral-domain optical coherence tomography in patients with pseudoexfoliation syndrome. *Eye*. 2015;29:791–796.
36. Cunha JP, Proença R, Dias-Santos A, et al. Choroidal thinning: Alzheimer's disease and aging. *Alzheimers Dement (Amst)*. 2017;8:11–17.
37. Alonso-Caneiro D, Read SA, Collins MJ. Automatic segmentation of choroidal thickness in optical coherence tomography. *Biomed Opt Express*. 2013;4:2795–2812.
38. Thomasy SM, Cortes DE, Hoehn AL, Calderon AC, Li JY, Murphy CJ. In vivo imaging of corneal endothelial dystrophy in Boston Terriers: a spontaneous, canine model for Fuchs' endothelial corneal dystrophy. *Invest Ophthalmol Vis Sci*. 2016;57:495–503.
39. Weiss JS, Møller HU, Lisch W, et al. The IC3D classification of the corneal dystrophies. *Cornea*. 2008;27:S1–S8.
40. Hutchings N, Simpson TL, Hyun C, et al. Swelling of the human cornea revealed by high-speed, ultrahigh-resolution optical coherence tomography. *Invest Ophthalmol Vis Sci*. 2010;51:4579–4584.

Investigative Ophthalmology & Visual Science

41. McNamara NA, Polse KA, Bonanno JA. Stromal acidosis modulates corneal swelling. *Invest Ophthalmol Vis Sci*. 1994;35:846–850.
42. Ettl AR, Felber SR, Rainer J. Corneal edema induced by cold. *Ophthalmologica*. 1992;204:113–114.
43. Wang J, Fonn D, Simpson TL, Jones L. Relation between optical coherence tomography and optical pachymetry measurements of corneal swelling induced by hypoxia. *Am J Ophthalmol*. 2002;134:93–98.
44. Arita R, Arita M, Kawai M, Mashima Y, Yamada M. Evaluation of corneal endothelial pump function with a cold stress test. *Cornea*. 2005;24:571–575.
45. Ross DH, Clark ME, Godara P, et al. RefMob, a reflectivity feature model-based automated method for measuring four outher retinal hyperreflective bands in optical coherence tomography. *Invest Ophthalmol Vis Sci*. 2015;56:4166–4176.
46. Litts KM, Zhang Y, Freund KB, Curcio CA. Optical coherence tomography and histology of age-related macular degeneration support mitochondria as reflectivity sources. *Retina*. 2018;38:445–461.
47. Curcio CA, Messinger JD, Sloan KR, Mitra A, McGwin G, Spaide RF. Human chorioretinal layer thicknesses measured in macula-wide, high-resolution histologic sections. *Invest Ophthalmol Vis Sci*. 2011;52:3943–3954.
48. Abbott CJ, McBrien NA, Grünert U, Pianta MJ. Relationship of the optical coherence tomography signal to underlying retinal histology in the tree shrew (Tupaia belangeri). *Invest Ophthalmol Vis Sci*. 2009;50:414–423.
49. Fischer MD, Huber G, Beck SC, et al. Noninvasive, in vivo assessment of mouse retinal structure using optical coherence tomography. *PLoS One*. 2009;4:e7507.
50. Anger EM, Unterhuber A, Hermann B, et al. Ultrahigh resolution optical coherence tomography of the monkey fovea. Identification of retinal sublayers by correlation with semithin histology sections. *Exp Eye Res*. 2004;78:1117–1125.
51. Schwagmeyer PL, Brown CH. Factors affecting male-male competition in thirteen-lined ground squirrels. *Behav Ecol Sociobiol*. 1983;13:1–6.
52. Salinas RY, Pearring JN, Ding JD, Spencer WJ, Hao Y, Arshavsky VY. Photoreceptor discs form through peripherin-dependent suppression of ciliary ectosome release. *J Cell Biol*. 2017;216:1489–1499.
53. Wilk MA, Huckenpahler AL, Collery RF, Link BA, Carroll J. The effect of retinal melanin on optical coherence tomography images. *Trans Vis Sci Tech*. 2017;6(2):8.
54. Zhang QX, Lu RW, Messinger JD, Curcio CA, Guarcello V, Yao XC. In vivo optical coherence tomography of light-driven melanosome translocation in retinal pigment epithelium. *Sci Rep*. 2013;3:2644.
55. Izatt JA, Choma MA. Theory of optical coherence tomography. In: Drexler W, Fujimoto JG, eds. *Optical Coherence Tomography: Technology and Applications*. Berlin, Heidelberg: Springer Berlin Heidelberg; 2008:47–72.
56. Tanna H, Dubis AM, Ayub N, et al. Retinal imaging using commercial broadband optical coherence tomography. *Br J Ophthalmol*. 2010;94:372–376.
57. Jonnal RS, Kocaoglu OP, Zawadzki RJ, Liu Z, Miller DT, Werner JS. A review of adaptive optics optical coherence tomography: technical advances, scientific applications, and the future. *Invest Ophthalmol Vis Sci*. 2016;57:OCT51–OCT68.

Investigative Ophthalmology & Visual Science